JOURNAL OF GEOPHYSICAL RESEARCH, VOL. 115, C05014, doi:10.1029/2009JC005457, 2010

Click Here for Full Article

# Mixed layer depth variability in the tropical boundary of the California Current, 1997–2007

Gilberto Jeronimo[1] and Jose Gomez-Valdes[2]

Received 20 April 2009; revised 11 November 2009; accepted 15 December 2009; published 19 May 2010.

[1] The variability of the mixed layer depth (MLD) is examined over a decade (1997–2007) for the tropical boundary of the California Current (24–32°N), using conductivity-temperature-depth observations collected by quarterly survey cruises. Results indicate that salinity gradients control MLD rather than temperature gradients. The mean state of the upper ocean indicates that contours of constant MLD are parallel to the coast, with mixed layer thickness decreasing toward the coastal zone. The deepest (~70 m) thickness is reached in January and the shallowest (~15 m) occurs in July. The warmer conditions (summer) are reproduced for a simple thermal energy equation. The rest of the seasons are reproduced for a one-dimensional momentum balance for the upper ocean, which includes Ekman dynamics and stratification. This comparison indicates that the variability of MLD is mainly due to wind-driven phenomena except during the heating period. In particular, seasonal and interannual variability of the MLD are correlated with offshore Ekman transport. An abrupt MLD change occurs between January 1998 and January 2000 associated with the strong El Niño-La Niña cycle shift that occurred in this period.

**Citation:** Jeronimo, G., and J. Gomez-Valdes (2010), Mixed layer depth variability in the tropical boundary of the California Current, 1997–2007, *J. Geophys. Res.*, *115*, C05014, doi:10.1029/2009JC005457.

## 1. Introduction

[2] In eastern boundary currents the temporal evolution of the upper waters is determined by atmosphere-ocean interactions and coastal ocean dynamics [*Lentz*, 1992]. Studies of the variability of the mixed layer depth (MLD) in such regions are therefore of a great importance to evaluate the effect of local and basin-scale changes in the upper ocean. In particular, low-frequency MLD changes in the northeast Pacific are related to large-scale atmospheric forcing on the Pacific Ocean. For example, *Polovina et al.* [1995] and *Freeland et al.* [1997] reported changes in the winter mixed layer related to the Alaska gyre circulation. Moreover, *Cummins and Lagerloef* [2002] found that long-term MLD variability is controlled by Ekman pumping. Observations in the California Current System by California Cooperative Oceanic Fisheries Investigations (CalCOFI) have also revealed long-term fluctuations in stratification. *Palacios et al.* [2004] reported interannual variations in thermocline depth and *Kim and Miller* [2007] found that the variability of the thermocline temperature has changed in the last 50 years.

[3] *Gomez-Valdes and Jeronimo* [2009, hereafter *GVJ*2009] used a 10 year Mexican Research of the California Current (IMECOCAL) data set to investigate the interannual variability of mixed layer (ML) temperature and salinity off Baja California. They found that ML temperature is controlled by local processes and ML salinity by basin-scale processes. Although they computed the isothermal layer and the isohaline layer depth to integrate the thermodynamic properties, they did not report the patterns of these layers.

[4] MLD is regularly calculated using density based criteria [*Schneider and Müller*, 1990; *Lukas and Lindstrom*, 1991; *Brainerd and Gregg*, 1995], although in some regions temperature based criteria are also valid [*Kara et al.*, 2003; *de Boyer Montegut et al.*, 2004]. In this report, we use the same *GVJ*2009 data set to describe for the first time the seasonal and interannual variability of MLD off Baja California. Because we find that isothermal layer depth is different from isohaline layer depth, we use a potential density criterion to estimate MLD. The prediction of the seasonal MLD changes is addressed with simple models. The influence of El Niño-Southern Oscillation (ENSO) on the interannual MLD variability is also addressed.

[5] A brief description of data and estimation methods of MLD are given in sections 2 and 3, respectively. In section 4, the seasonal MLD changes are analyzed using simple models. Seasonal and interannual variability of the MLD via empirical orthogonal functions (EOFs) analysis are given in sections 5 and 6, respectively. Correlation analysis of forcing mechanisms and climatic indices are also presented in

[1]UMDI-Sisal, Facultad de Ciencias, UNAM, Sisal, Mexico.
[2]Physical Oceanography Department, CICESE, Ensenada, Mexico.

Copyright 2010 by the American Geophysical Union.
0148-0227/10/2009JC005457

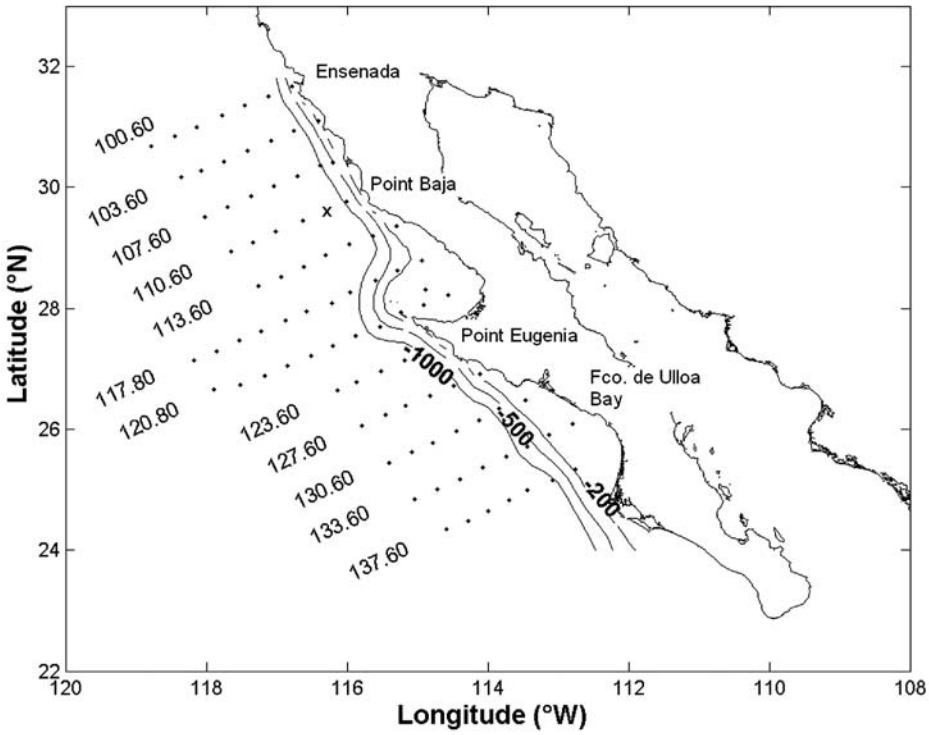


**Figure 1.** IMECOCAL station plan. Core measurements at each station consist of CTD/Rosette cast and an oblique bongo net tow. The black cross indicates the location of station 110.40. Depth contours are in m.

sections 5 and 6. In section 7, a discussion of the observations is elaborated.

## 2. Data

[6] Our data set originated from 36 quarterly hydrographic surveys, which were carried out from October 1997 to January 2007 off Baja California, as part of the monitoring program of IMECOCAL. More information about this program is given by *Baumgartner et al.* [2008]. The sampling grid of the surveys covered 12 hydrographic lines spaced 74 km apart (Figure 1), with stations (black points) spaced 37 km apart. Mostly, in each station conductivity-temperature-depth (CTD) casts were taken from the surface to 1 000 m depth, although deeper casts were also taken. Following California Cooperative Oceanic Fisheries Investigations (CalCOFI) program, station locations were designed by a line and station number; e.g., 110.40 is station 40 on line 110, which is located due west of northern Baja California. Data were linearly interpolated to a 1 dbar interval. Temperature and conductivity sensors were factory calibrated prior to each survey.

## 3. Estimation of MLD

[7] To calculate the isopycnal layer depth (MLD) we used the methodology of *Kara et al.* [2000, hereafter *K*2000]. Similar to *K*2000, we defined MLD as the distance of the quasi-isopycnal layer from reference level to the level where density has changed by a fixed $\Delta\sigma_\theta = \sigma_\theta(\theta + \Delta\theta, S, P) - \sigma_\theta(\theta, S, P)$, where S is salinity, P is pressure (=0), and $\Delta\sigma_\theta$ is a potential density increment. To avoid the effect of seawater compressibility on the estimation of MLD, following *Schneider and Müller* [1990] and *Brainerd and Gregg* [1995] we used potential temperature ($\theta$) and potential density ($\sigma_\theta$), while *K*2000 used T and $\sigma_T$.

[8] The method of *K*2000 requires determination of an optimal $\Delta\theta$ value. To determine the best $\Delta\theta$ value, a subjective (visual) estimation of the layer depths was carried out directly from eight cruises. The root mean square error (RMSE) between visual estimation and *K*2000 method was used to choose the best $\Delta\theta$. The optimal value was time dependent. Optimal $\Delta\theta$ was 0.2°C for April, a $\Delta\theta$ = 0.5°C for July, and $\Delta\theta$ = 0.8°C for October and January. Average value of RMSE for the whole period was about 3.0 m, with the minimum value occurring in October.

[9] After calculating MLD for all vertical profiles, we constructed the respective two dimensional fields, following the methodology elaborated by *Jeronimo and Gomez-Valdes* [2006] for optimal interpolation. We calculated the correlation scales for the x-y (across and along coast) plane, resulting ~70 km in x direction and ~120 km in y direction. By error minimization conditions, the distance between adjacent points on the grid was chosen equal to 18 km. The mean and the standard deviation of the mean (standard error) of the gridded data were calculated from 34 of 36 surveys, since we did not include October 1997 and January 1998 to avoid bias of the estimator by the strong 1997–1998 El Niño [*McPhaden*, 1999].

[10] Figure 2 shows mean and standard error distributions of MLD. To describe the fields, we adopted *Lynn and Simpson*'s [1987] domain partition definition, who divided the California Current System in three zones: coastal, transition, and oceanic. However, the hydrographic sampling of

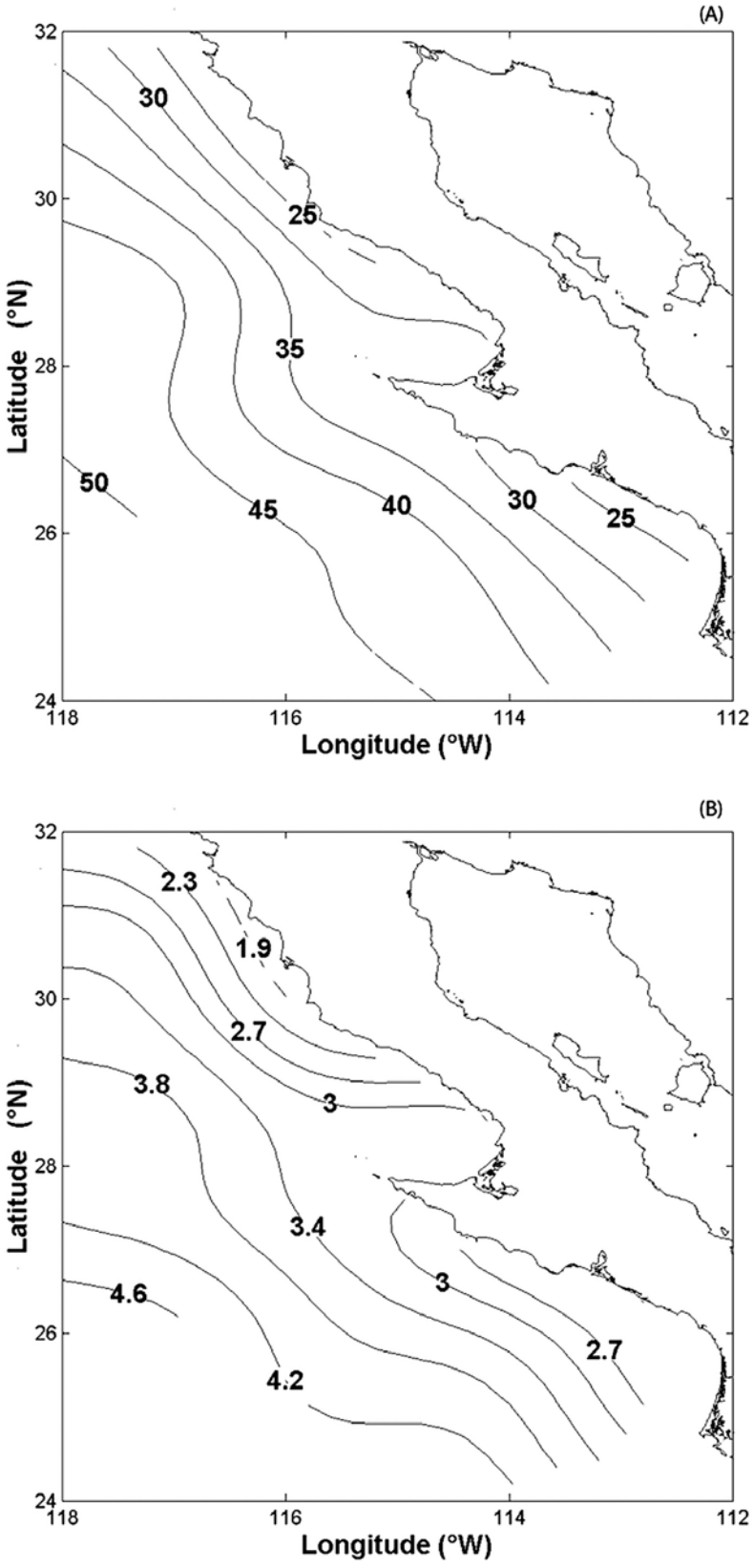


**Figure 2.** Spatial patterns of (a) mean and (b) standard error of the isopycnal layer depth (MLD) for IMECOCAL sampling grid. Units are in m.

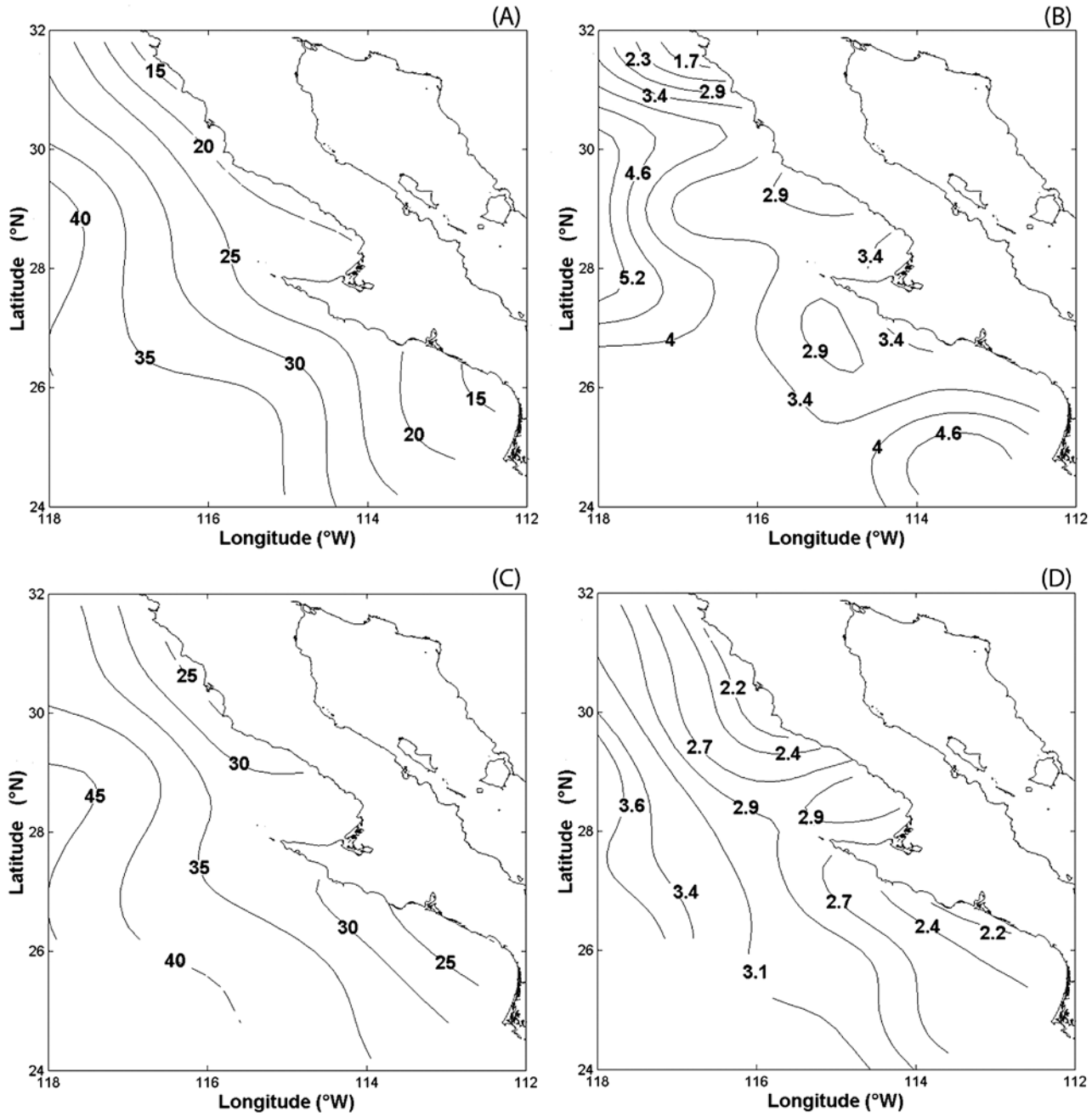


**Figure 3.** The same as Figure 2 but for (a and b) isothermal and (c and d) isohaline layer depth.

IMECOCAL is restricted to the first two zones. Contours of constant mean are parallel to the coast (almost meridional orientation) and the mean thickness is shallower in the coastal zone than in the transition one. The spatial range is 25 m. The minimum thickness (20 m) occurs in the coastal zone off northern Baja California (north of 28°N). Contours of constant standard error (variability) are also in meridional orientation. The variability of the mean MLD is smaller in the coastal zone than in the transition one.

### 3.1. Comparison With Other Methods

[11] Searching for the most efficient method to calculate MLD in the tropical boundary of the California Current, we also examined the differences between isothermal and isohaline layer depth, since it is relatively easy to calculate MLD from these layers [*GVJ*2009]. Figure 3 shows the spatial structure of the mean and standard error of isothermal and isohaline layer. Contours of constant mean are parallel to the coast and the layers are shallower in the coastal zone. However, there are significant differences between the structures of the two layers. For example, isothermal layer depth is shallower and shows a higher variability than isohaline layer depth. Furthermore, contours of constant standard error are less meridional for the isothermal layer depth case than for the isohaline layer depth. It is

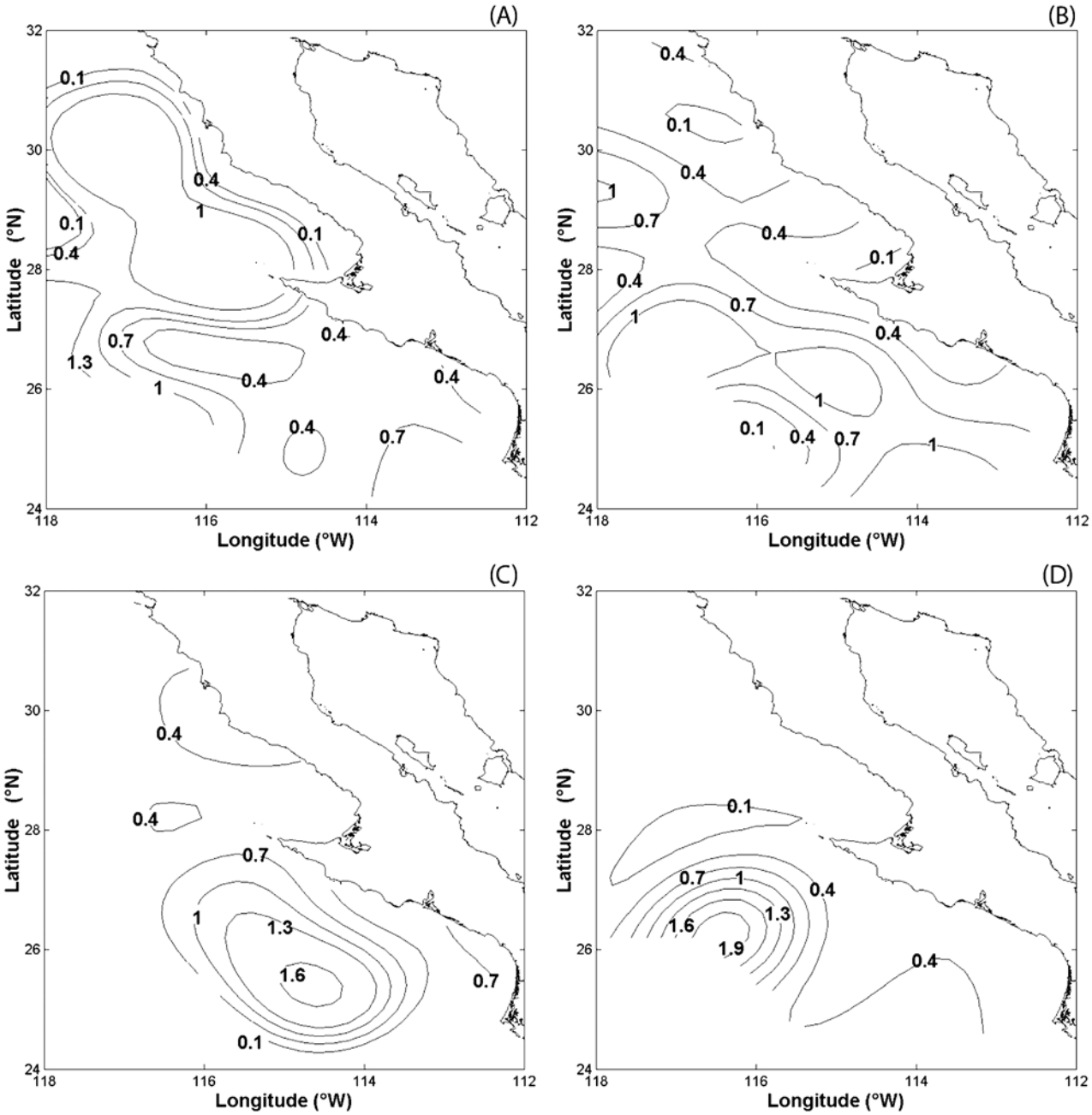


**Figure 4.** Seasonal changes of the relative importance of temperature and salinity on density: (a) January, (b) April, (c) July, and (d) October. Nondimensional values greater than 1 indicate dominance of temperature over salinity.

noteworthy the similarity between the spatial distribution of MLD and of isohaline layer depth, which indicates that salinity variations, rather than temperature variations, control MLD changes.

### 3.2. Relative Contributions of Temperature and Salinity on Density

[12] To assess the relative importance of temperature and salinity variations on density, we calculated $\beta\Delta\theta$ and $\alpha\Delta S$, where $\beta$ and $\alpha$ are the expansion coefficients of temperature potential and salinity [*Rudnick and Ferrari*, 1999]. $\Delta\theta$ and $\Delta S$ were calculated from 10 m depth to the MLD. Figure 4 shows the seasonal variation of $\beta\Delta\theta/\alpha\Delta S$ (density ratio). These patterns demonstrated the dominance of salinity gradients on density. The time/space patterns are associated to the seasonal cycle of the circulation patterns off Baja California [*Lynn and Simpson*, 1987] rather than to the Net Heat Flux (NHF) or precipitation-evaporation cycles [*Roden*, 1975].

[13] For example, two typical vertical profiles of temperature, salinity and density ($\sigma_\theta$) near the shelf break waters off northern Baja California area (station 110.40) are shown

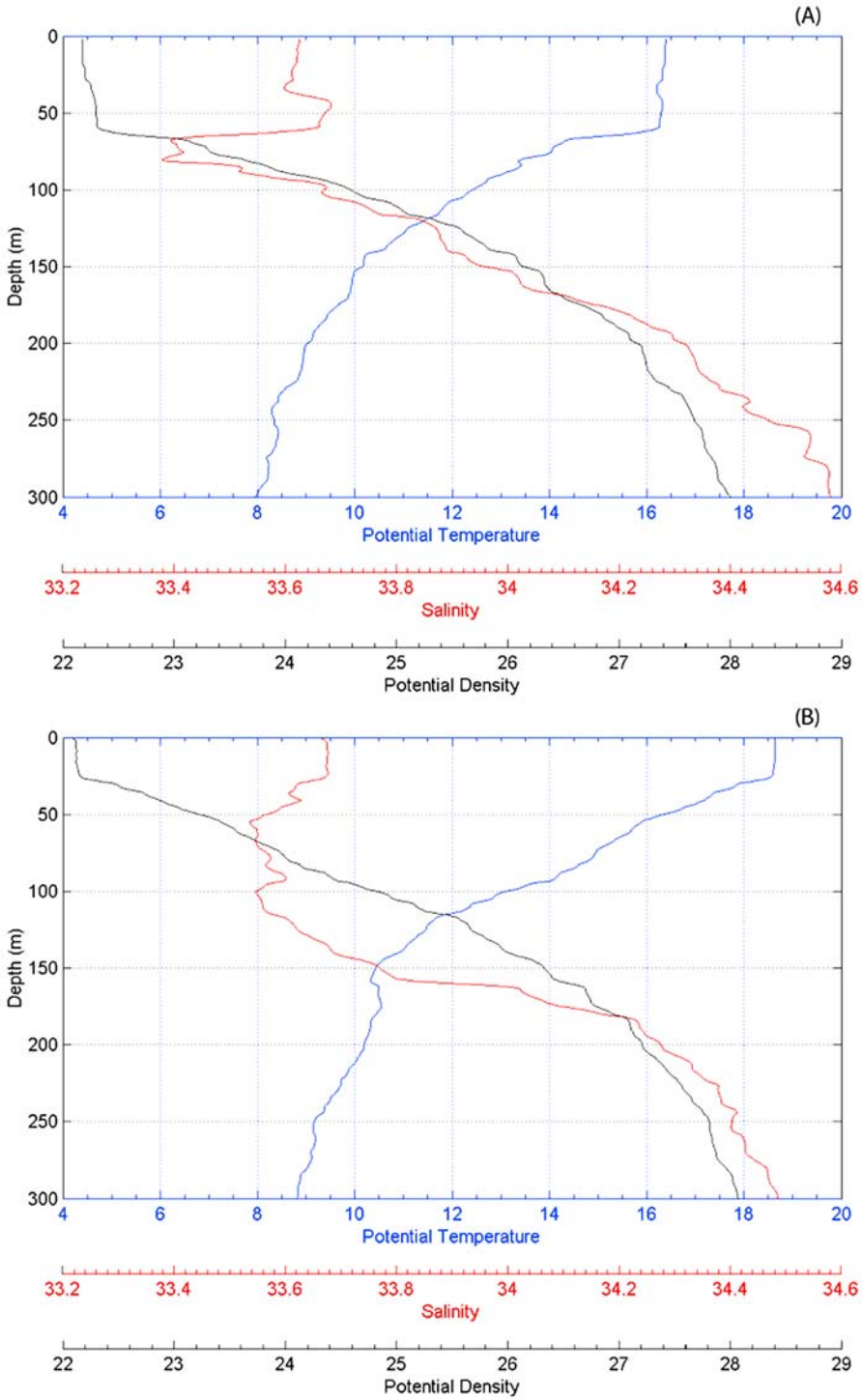


**Figure 5.** Vertical profiles of temperature, salinity, and density in offshore waters of line 110: (a) January and (b) July 2000. Temperature is in °C and density ($\sigma_\theta$) is in kg m$^{-3}$.

in Figure 5. During winter (January 2000) the MLD is deeper than the isothermal layer, due to the effect of the Inshore Countercurrent (salty and warm waters). Below of MLD is the layer of the minimum of salinity, which is associated with the California Current [*Reid et al.*, 1958]. During summer (July 2000) isopycnal and isothermal layer have almost the same depth. The signature of the California Current below the mixed layer is also evident here. The layer of minimum of salinity is also reported by *Barton and Argote* [1980] and *Jeronimo and Gomez-Valdes* [2007].

[14] In sections 3.1 and 3.2, we have demonstrated that to estimate MLD in the IMECOCAL region it is necessary to use a density criterion. However, besides *K*2000 method different approaches may be used to apply a density criterion. For

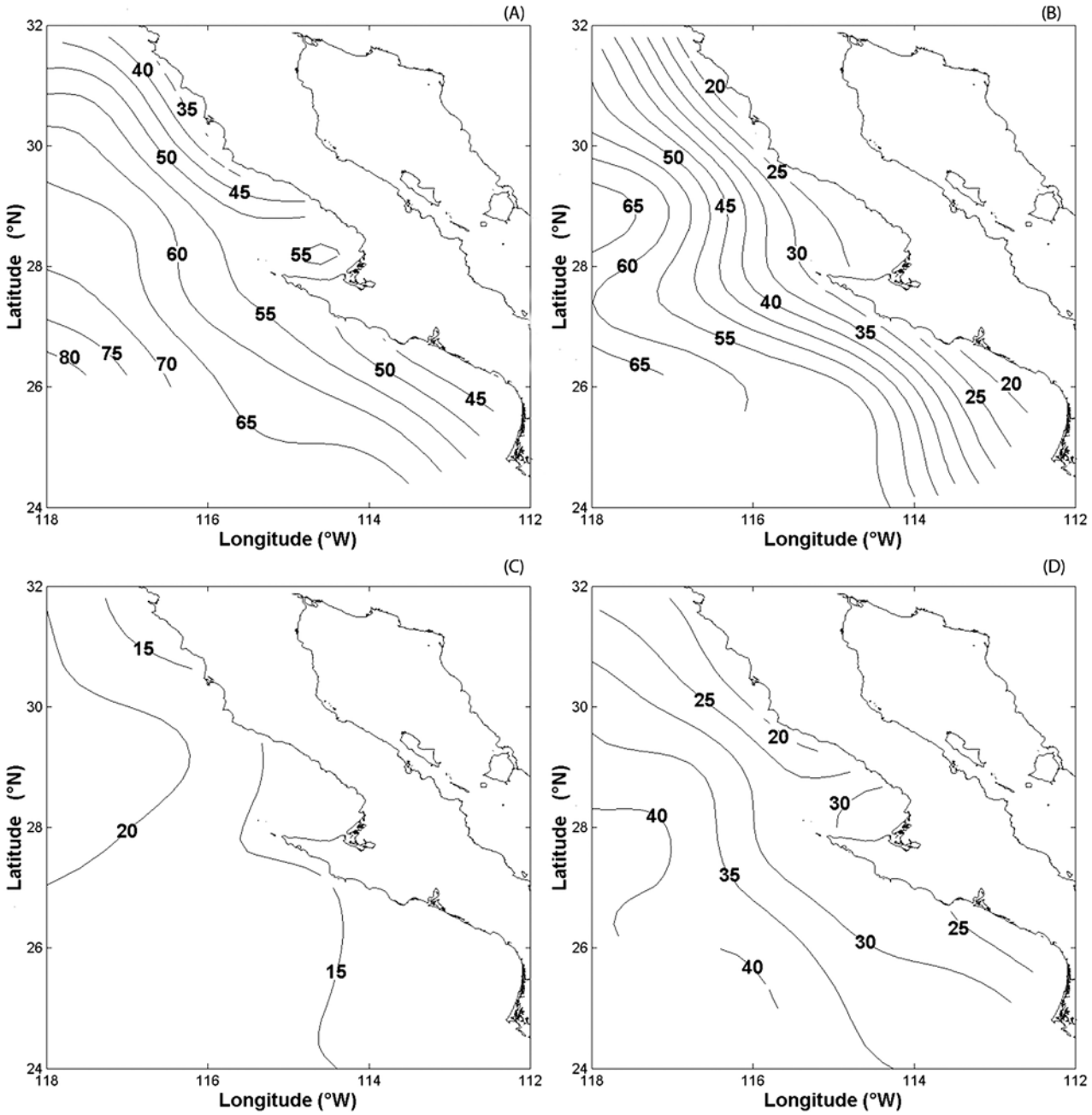


**Figure 6.** Seasonal MLD changes: (a) January, (b) April, (c) July, and (d) October. Units are in m.

comparison purposes, the method of *Sprintall and Tomczak* [1992] was also implemented for all CTD lances. The *Sprintall and Tomczak* [1992] method is also a threshold method, but it requires the calculation of thermal expansion coefficients in each profile. The relationship between the two approaches was found to be linear, $y = 1.01\ x - 0.79$. The overall mean difference between the two methods was ~ 3 m, about the level of significance of MLD.

## 4. Mean Seasonal MLD Changes

[15] Since two independent approaches to calculate MLD from density profile gave the same results, we are confident that our MLD determination is not method dependent. In the rest of the paper, MLD results using the *K*2000 method are discussed.

[16] To illustrate mean seasonal MLD changes, we used a harmonic analysis model via a least squares fit. The general form of the model is

$$MLD = A_0 + \{A_1(\vec{x})\cos(\varphi_1 t - f_1) + A_2(\vec{x})\cos(\varphi_2 t - f_2)\}, \quad (1)$$

where $A_0$ stands for the mean of the time series at each station, the second rhs term is the mean seasonal component of the MLD, where $A_1$ and $A_2$ are the annual and semiannual amplitudes for each time series, respectively, $\phi_1$ and $\phi_2$ are the frequency of annual and semiannual harmonics, $f_1$ and $f_2$ are the phase of annual and semiannual harmonics, and $t$ is

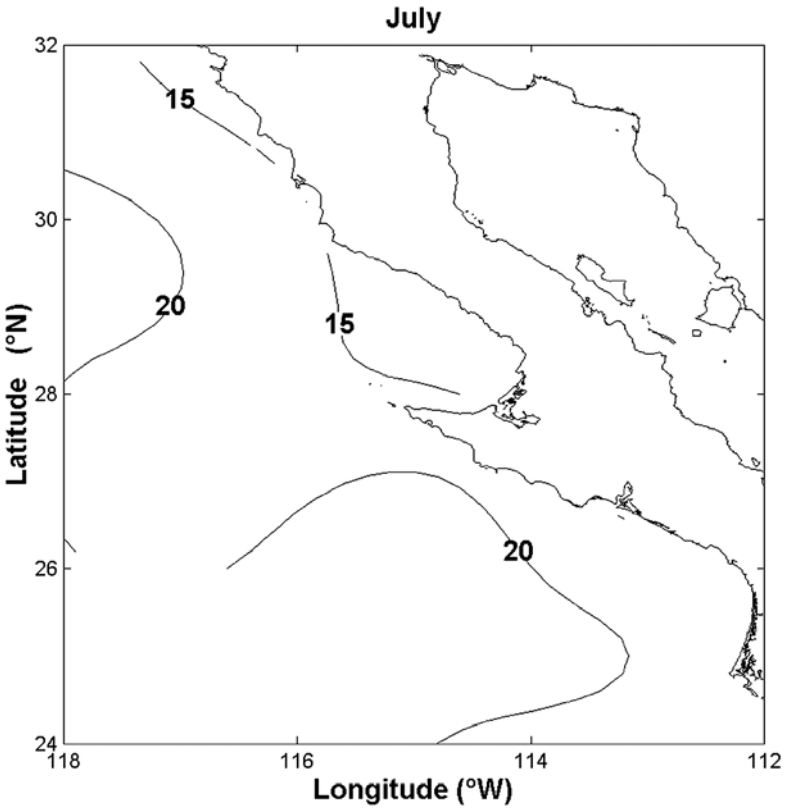


**Figure 7.** *Kraus and Turner*'s [1967] model results for July.

time. The explained variance for the model was computed in the form

$$V_j = \frac{|A_j(\vec{x})|}{\sum_{i=0}^{2} |A_i(\vec{x})|}, \tag{2}$$

where $j$ is an entire that represent the mode.

[17] The explained variance for the harmonic model was higher in the coastal zone (50%) than in the transition one (46%). Figure 6 shows the seasonal MLD changes off Baja California. In general, contours of constant thickness are parallel to the coast and MLD is shallower in the coastal zone than in the transition one. The coast-ocean gradient is stronger during April than in the rest of the year, when the northwest winds are strong and parallel to the coast [*Perez-Brunius et al.*, 2007]. The maximum thickness (80 m) occurs in January and the minimum (15 m) in July, following the NHF cycle in the northeastern Pacific [*Moisan and Niiler*, 1998]. There is an obvious difference between the coastal zone of northern and of southern (south of 28°N) Baja California; in the northern zone the coast-ocean gradient is stronger than in the southern particularly in January and October. These features appear to be related to local circulation patterns off northern Baja California [*Barton and Argote*, 1980; *Strub and James*, 2000; *Jeronimo and Gomez-Valdes*, 2007].

[18] Such results suggest that seasonal MLD changes off Baja California are determined not only by ocean-atmosphere interactions but also by ocean dynamics. To evaluate the relative importance of these processes two simple models for the upper ocean were implemented. The bulk mixed layer model of *Kraus and Turner* [1967], governed by the thermal budget equation, allows the evaluation of the relative importance between heat fluxes and wind stress forcing. On the other hand, the *Pollard et al.* [1973] model permits the evaluation of the relative importance between Ekman dynamics and stratification [*Lentz*, 1992].

### 4.1. One-Dimensional Model of *Kraus and Turner* [1967]

[19] Mixed layer or bulk models assume that temperature, salinity and horizontal velocity are uniform within the layer. *Kraus and Turner* [1967] proposed simple models to predict layer depth of the upper ocean due to heat exchanges between the atmosphere and the ocean. During the heating period the entrainment of the lower fluid into the mixed layer is negligible [*Niiler and Kraus*, 1977] and, therefore, the mixed layer and the ocean interior are decoupled and the physics is simplified.

[20] The *Kraus and Turner* [1967] model to predict mixed layer depth ($h_m$) for the heating period is

$$h_m = \frac{2m_* \rho_s C_p}{g\alpha} \frac{u_*^3}{Q}, \tag{3}$$

where $m_*$ is a parameter, $u_*^2 = \tau/\rho$ is friction velocity, $\tau$ is wind stress, $\rho$ is density of the ocean surface layer, $g$ is gravity, $\alpha$ is the coefficient of thermal expansion, $\rho_s$ is air density, $C_p$ is heat capacity, and $Q$ is buoyancy flux (heat).

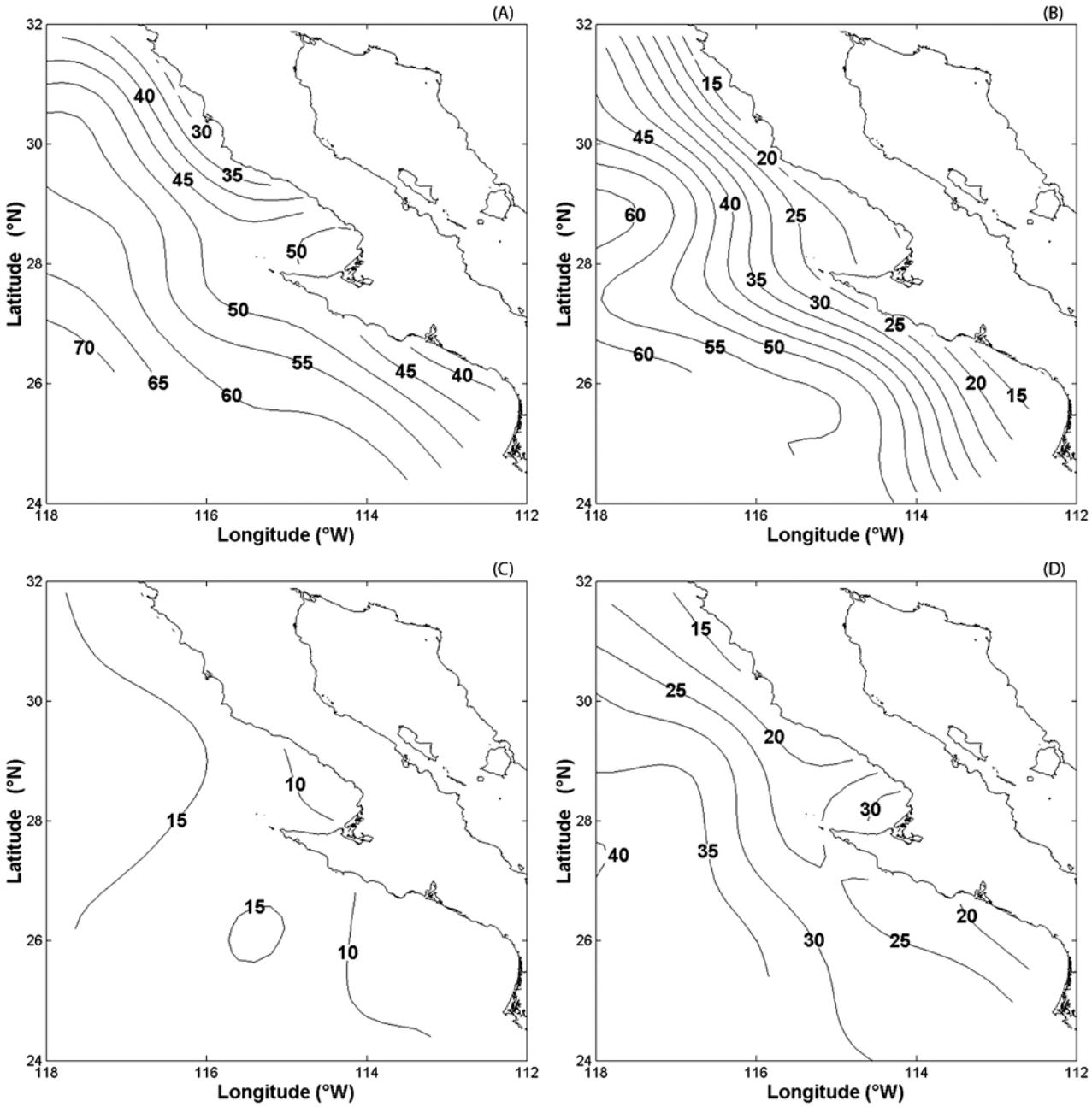


**Figure 8.** *Pollard et al.*'s [1973] model results: (a) January, (b) April, (c) July, and (d) October. Units are in m.

[21] The model was run for each grid point using $m_* = 7.5$, $g = 9.81\ ms^{-2}$, $\alpha = 2.5 \times 10^{-4}\ ^{\circ}C^{-1}$, and $C_p = 3988\ Jkg^{-1}C^{-1}$. The wind-forcing term $\tau^s = \sqrt{\tau_x^2 + \tau_y^2}$ was calculated from QuikScat wind velocity data following *Hasse and Smith* [1997]. The buoyancy flux forcing term was obtained from NCEP/NCAR reanalysis project. It was calculated from $Q = Q_B + Q_s - Q_I + Q_L$, where $Q_B$ is long wave radiation, $Q_S$ is sensible heat flux, $Q_I$ is short wave radiation, and $Q_L$ is the latent heat flux term. Figure 7 shows the output of the *Kraus and Turner* [1967] model for July. The model reproduces very well the MLD observed values for this period. The overall root mean square error between model and observed values was 1.5 m.

[22] We also carried out an experiment using *Kraus and Turner*'s [1967] model for both the heating and the cooling periods (not shown). The model reproduced the observed MLD values for the heating season (July) as expected. However, for the rest of the seasons the overall performance of the model was low.

### 4.2. One-Dimensional Model of *Pollard et al.* [1973]

[23] *Pollard et al.*'s [1973] model is a one-dimensional dynamical balance among acceleration, Coriolis and viscous terms. It represents a balance between shear-generated turbulence at the base of the mixed layer and an increase in the potential energy due to entrainment of the denser interior

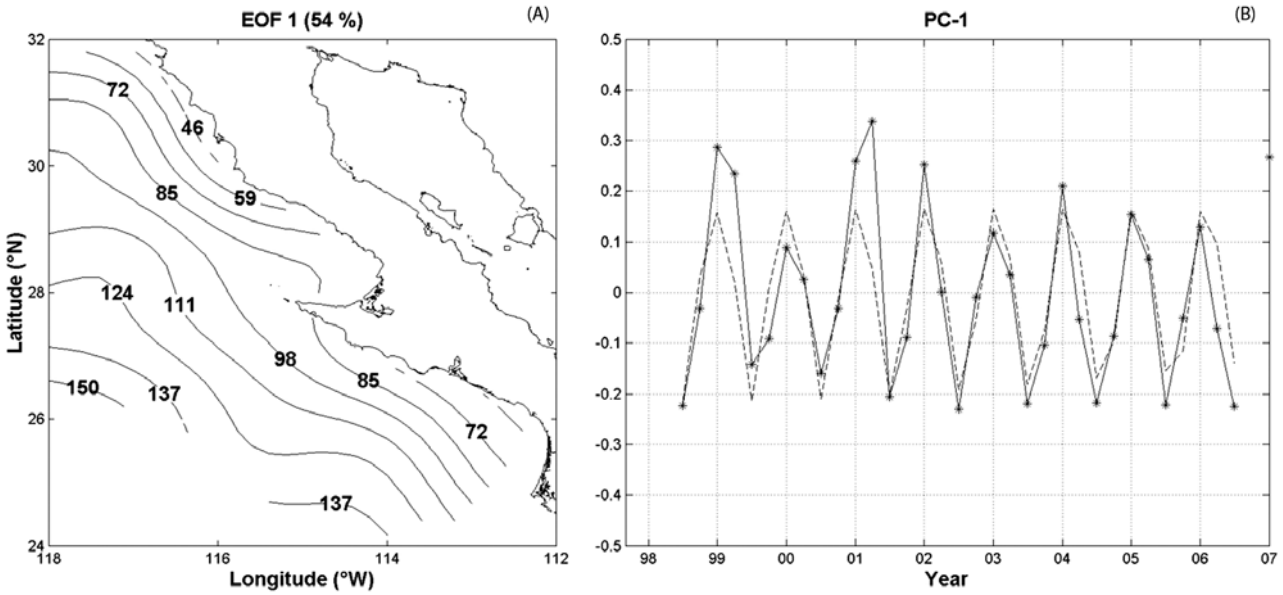


**Figure 9.** (a) The spatial pattern and (b) the principal component of the first leading EOF of quarterly MLD anomalies. Units are in m.

water into the mixed layer [*Lentz*, 1992]. The mixed layer depth predicted by the model of *Pollard et al.* [1973] for $Q = 0$ is calculated by

$$MLD_{PRT} = \frac{Au_*}{\sqrt{N_1 f}}, \tag{4}$$

where $u_* = \sqrt{\frac{\tau^s}{\rho_0}}$ is shear velocity, $\tau^s$ is wind stress magnitude, $\rho_0$ is the reference density, $N_1$ is the buoyancy frequency just below the mixed layer, $f$ is the Coriolis parameter, and $A$ is a proportionality constant.

[24] The model was run for each grid point using $\rho_0 = 1024\ \mathrm{kgm}^{-3}$, $f$ was calculated for each latitude ($f = 2 \times 7.292 \times 10^{-5} \times$ latitude $s^{-1}$), $N_1 = 2.8881 \times 10^{-4}\ \mathrm{s}^{-1}$, and $\tau^s = \sqrt{\tau_x^2 + \tau_y^2}$, was calculated from QuikScat wind velocity data following *Hasse and Smith* [1997]. Density and buoyancy frequency references were calculated using CTD data set. We found that the optimal value for the proportionality constant was $A = 1.7$, in agreement with those reported by *Pollard et al.* [1973] and *Lentz* [1992].

[25] Figure 8 shows $MLD_{PRT}$ for January, April, July, and October. The model reproduces very well the seasonal MLD changes in the entire domain. The overall root mean square error between model and observed values was ~ 1.5 m for January, 1.0 m for April, 2.0 m for July, and 1.5 m for October. It is also noteworthy that the model output does resemble the observed values everywhere; in particular, this model predicts the strong coast-ocean gradient in April. In contrast, *Lentz* [1992] found that this model reproduced MLD adequately only during the upwelling season in eastern boundary current.

## 5. Seasonal Variability

### 5.1. MLD

[26] In this section, the seasonal variability of MLD is addressed. To extract the spatial and temporal variability of MLD, the method of EOFs was applied to the gridded data [*Wunsch and Heimbach*, 2009]. The mean was removed from the time series in each grid point to construct quarterly anomalies in the form

$$MLD_i' = MLD_i - \frac{1}{N}\sum_{t=1}^{N} MLD_t, \tag{5}$$

where $N$ is the number of cruises.

[27] EOFs analysis of $MLD'$ was carried out for $N = 34$, not including the 1997–1998 El Niño surveys, namely October 1997 and January 1998. Although according to the sampling criteria of *North et al.* [1982] the first two modes were well separated, we restrict our presentation to the spatial and temporal patterns of the first leading mode, which captured most of the variability. EOF-1 (first leading mode) accounts for 54% of total variance (Figure 9). The spatial pattern shows a single-signed loading, in which variability increases monotonically seaward. This pattern is similar to the standard error map (Figure 2b). Its corresponding principal component (PC) time series shows a strong annual cycle (dashed line) in which the maximum positive occurs in January and the minimum negative in July. This mode evidently represents the predominant annual cycle in MLD variability.

[28] We also carried out an experiment with the 1997–1998 El Niño cruises (not shown). The differences between both experiments were quantitative rather than qualitative. EOF-1 accounted for 78%, but the variability structure remained largely the same.

### 5.2. Forcing Mechanisms

[29] Because the *Pollard et al.* [1973] model indicates that the wind is an important forcing term in the determination of MLD, we now decompose the wind stress field into two orthogonal components. Here we present the analysis of $\tau^y$ the parallel to the coast component and $\tau^x$ the perpendicular

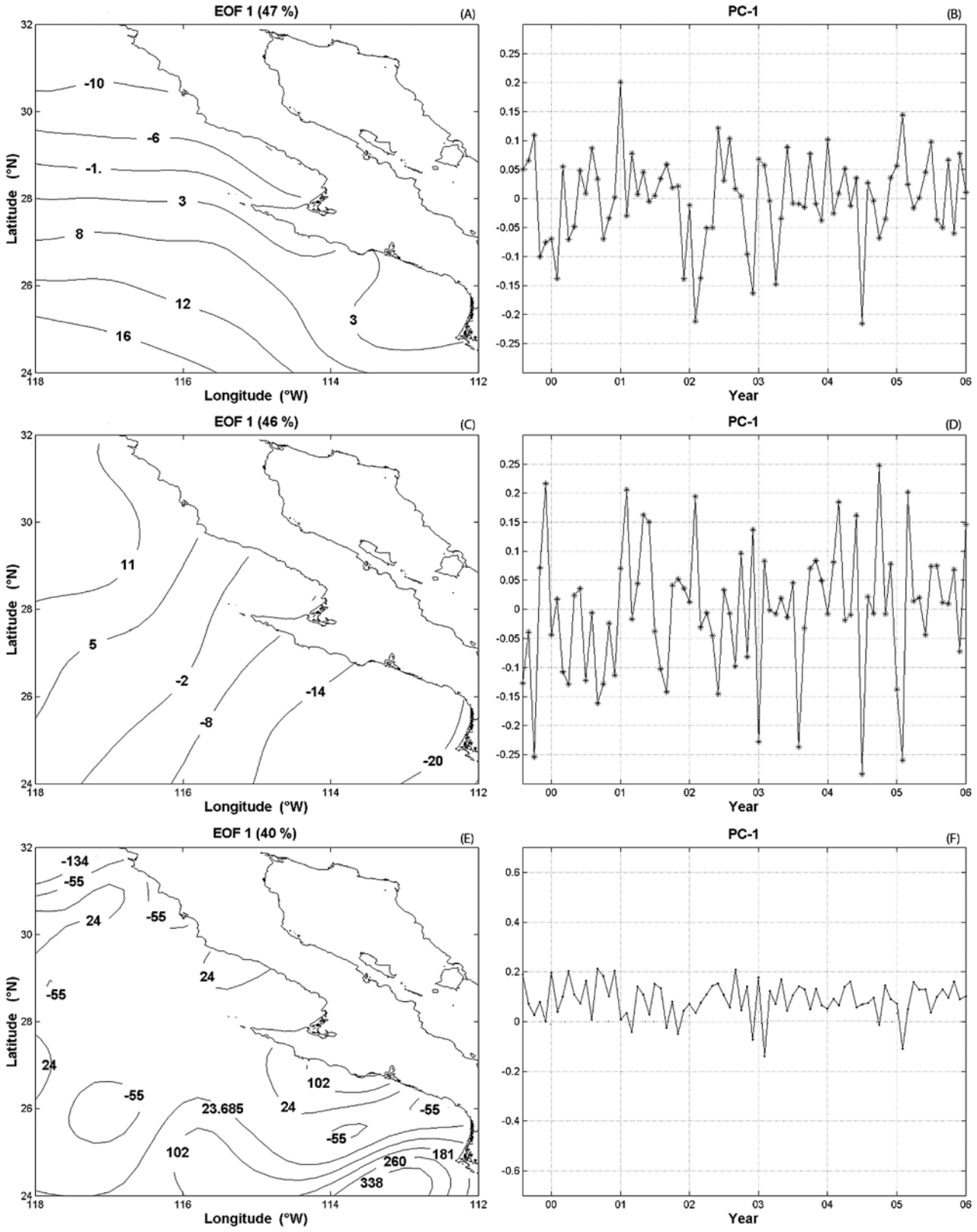


**Figure 10.** The spatial and temporal patterns of the first leading EOF of quarterly anomalies: (a and b) $\tau^y$, (c and d) $\tau^x$, and (e and f) for Ekman pumping. Units are in $Nm^{-2}$ for wind stress components and $ms^{-1}$ for Ekman pumping.

**Table 1.** Correlation Coefficient Between PC of the First Leading Mode of the Quarterly MLD Anomalies and PC of the First Three Leading Modes of Each Forcing Term

| | | Forcing Term Leading Mode | | |
|---|---|---|---|---|
| | MLD Leading Mode | 1 | 2 | 3 |
| Wind stress $x$ | 1 | 0.3 | 0.4 | 0.1 |
| Wind stress $y$ | 1 | −0.4 | −0.4 | 0.3 |
| Ekman pumping | 1 | 0.2 | 0.2 | −0.5 |

to the coast component. For completeness, we also present the analysis of Ekman pumping ($w_e$). The wind stress components are related to the mass transport in the Ekman layer [*Salmon*, 1998] in the form

$$f \int_{-D}^{0} \rho u \, dz = \tau^y; \quad f \int_{-D}^{0} \rho v \, dz = -\tau^x, \tag{6}$$

where $f$ is the Coriolis parameter, $D$ is Ekman depth, $\rho$ is density, $u$ is zonal velocity component, $v$ is meridional velocity component, $z$ is vertical direction. Ekman pumping was calculated from the wind stress curl and the variation of the Coriolis parameter, in the form

$$w_e = \frac{1}{\rho f}\left[\hat{z} \cdot \nabla \times \vec{\tau} + \frac{\beta \tau^x}{f}\right], \tag{7}$$

where $\rho$ is density (constant), $f$ is Coriolis parameter, $\hat{z}$ is the unit vector in vertical direction, $\vec{\tau}$ is the wind stress vector, $\beta$ is the variation of $f$ with latitude and $\tau^x$ is the x component of the wind stress. $\tau^y$, $\tau^x$ and $w_e$ were calculated from QuikScat wind velocity following *Hasse and Smith* [1997]. EOFs analysis of these forcing mechanisms was carried out basically using the same methodology as for EOFs analysis of *MLD′*.

[30] The surface circulation in the northeast Pacific is driven by winds generated by a high and a low atmospheric pressure system [*Reid et al.*, 1958]. The location of these cells changes significantly at seasonal and interannual timescales [*Reid et al.*, 1958; *Murphree and Reynolds*, 1995]. Thus, EOFs of the forcing terms might capture the variability of the cells. Figure 10 shows the first leading modes of $\tau^y$, $\tau^x$ and $w_e$. EOF-1 of $\tau^y$ accounts for 47% of total variance, its spatial variability shows a double-signed pattern, which separates the variability into north and south regions off Punta Eugenia, contours of constant variability are zonal. Its PC amplitude is generally high in winter and low in summer. EOF-1 of $\tau^x$ accounts for 46% of total variance, its spatial variability shows a double-signed pattern also, where contours of constant variability are perpendicular to the coast. Its PC amplitude is generally high in winter and low in spring. While EOF-1 of $w_e$ accounts for 40% of total variance, its spatial variability is patchy, with a region of high variability off southern Baja California. Its PC amplitude is single signed, predominantly positive.

### 5.3. Correlation Analysis

[31] Table 1 shows the correlation coefficients between PC of *MLD′* and PC of forcing mechanisms. According to *Emery and Thomson* [2001], correlation values ($r$) greater than 0.35 are significant at the 95% level. In this analysis, we presented correlation values for the three first leading modes of each forcing mechanism because according to the sampling criteria of *North et al.* [1982] they were well separated. The leading modes of $\tau^y$ are significantly correlated with the leading mode of *MLD′*, which indicates that offshore Ekman transport is controlling the *MLD′* variability. Alongshore Ekman transport and Ekman pumping have a lower-order effect on the *MLD′* variability.

[32] Taking into account the good performance of *Pollard et al.* [1973] model, we made two experiments with the

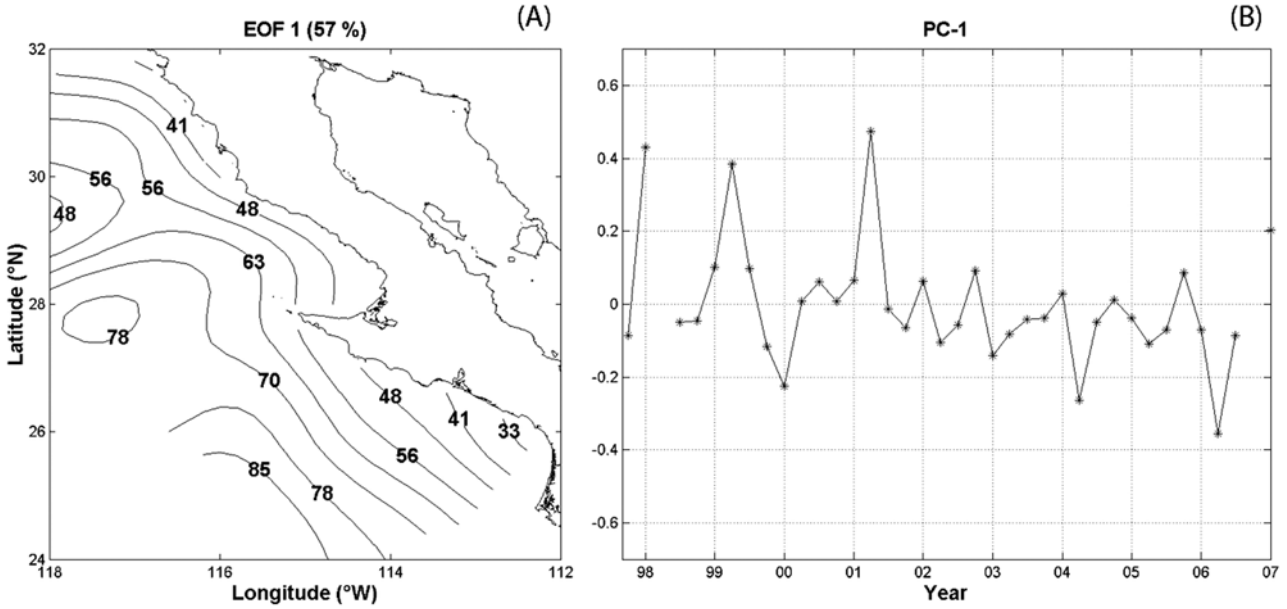


**Figure 11.** The same as Figure 9 but for interannual MLD anomalies.

**Table 2.** Correlation Coefficient Between PC of The First Leading Mode of the Interannual MLD Anomalies and PC of the First Three Leading Modes of Each Forcing Mechanism

| | | Forcing Mechanism Leading Mode | | |
|---|---|---|---|---|
| | MLD Leading Mode | 1 | 2 | 3 |
| Wind stress $x$ | 1 | 0.2 | −0.2 | 0.1 |
| Wind stress $y$ | 1 | −0.5 | 0.3 | 0.2 |
| Ekman pumping | 1 | 0.2 | 0.1 | 0.1 |

same parameters used in the model for the simulation of the seasonal MLD changes except the wind stress term (not shown). Instead of use the norm of the wind stress vector, we used the norm of $\tau^y$ in the first experiment and the norm of $\tau^x$ in the second one, where both components were computed as above described. We found that the relative importance between $\tau^y$ and $\tau^x$ in the determination of MLD was higher for the former than for the latter for a factor 2–3. These experiments validate the results of the correlation analysis.

## 6. Interannual Variability

### 6.1. MLD

[33] To analyze the nonseasonal (interannual) variability, the seasonal anomalies were subtracted from the lhs term of the equation (5), in the form

$$MLD'' = MLD' - \{A_1(\vec{x})\cos(\varphi_1 t - f_1) + A_2(\vec{x})\cos(\varphi_2 t - f_2)\}. \quad (8)$$

The spatial pattern of EOF-1 (Figure 11) is similar to the corresponding leading mode using quarterly anomalies. It accounts for 57% of the total variance. The PC amplitude shows clearly the event 1997–1998 El Niño, in January 1998 the MLD was anomalously high (deeper). It is noteworthy that the variability in this mode is stronger in the period 1997–2002 than in the period 2002–2006, which is due to the high amplitude of the *MLD′* anomalies during, January 1998, April 1999, and April 2001. This period correspond to the El Niño-La Niña cycle [*Meinen and McPhaden*, 2000]. During spring, the northwest winds are the strongest of the year off Baja California [*Perez-Brunius et al.*, 2007], which tends to push the current along. Thus, the spikes in April might be related to anomalous high winds. *Murphree and Reynolds* [1995] suggested than during La Niña conditions the equatorward wind is anomalously high over the northeast Pacific. The 1999–2001 La Niña events over the northeast Pacific [*Bograd et al.*, 2000; *Schwing et al.*, 2002] might be the cause of the deepening of the mixed layer.

[34] A sensitivity EOFs analysis was also performed on the interannual anomalies excluding April 2001, when the amplitude is maximum. The patterns above described were basically the same.

### 6.2. Forcing Mechanisms

[35] We also carried out EOFs analysis of $\tau^y$, $\tau^x$ and Ekman pumping forcing terms from its interannual anomalies following the same procedure as for *MLD′*. We found that the variability patterns for interannual anomalies were similar to the variability patterns for the seasonal anomalies shown in section 5. Table 2 shows the correlation coefficients between PC of the first leading *MLD″* mode and PC of the forcing mechanisms. *MLD″* variability is only significantly correlated with offshore Ekman transport variability. It is noteworthy that *MLD″* does not respond to Ekman pumping has in other regions does it, e.g., at Ocean Weather Station P [*Cummins and Lagerloef*, 2002].

### 6.3. Climate Indices

[36] To investigate the effect of low-frequency process on *MLD″* variability, correlation analysis was performed not only with interannual anomalies of the forcing terms but also with large-scale climate indices such as Pacific Decadal Oscillation (PDO) [*Mantua et al.*, 1997], Warm Water Volume (WWV) anomaly [*Meinen and McPhaden*, 2000], and NPGO [*Di Lorenzo et al.*, 2008]. Table 3 shows correlation coefficients between the temporal patterns (PC) of *MLD″* variability and climate indices. PDO is not correlated with *MLD″* variability. WWV is significantly correlated with PC-1, which implies that ENSO has the dominant long-term oscillation on *MLD″* variability. Nevertheless, NPGO is significantly correlated with PC-2 of *MLD″* (not shown).

## 7. Discussion

[37] The temporal evolution of MLD off Baja California has been presented for the first time. Because isothermal and isohaline layer depth are different from each other, it was necessary to use a criterion based in the potential density profile to estimate MLD. Isohaline layer depth followed MLD more closely, due to predominant steering of salinity variations on density variations. We hypothesized that in the IMECOCAL domain the mixed layer is mainly controlled by wind-driven phenomena except during the heating season.

[38] The mean state of MLD showed a coast-ocean gradient with the shallowest part at the coast. This pattern suggests that coastal ocean dynamics is an important factor in the determination of the MLD. For example, the alongshore wind stress component drives offshore Ekman transport which generates a sloping thermocline [*Lentz*, 1992]. MLD follows the 25 $\sigma_\theta$ isopycnal surface [*Jeronimo and Gomez-Valdes*, 2006], which shows an upward tilt toward the coast off northern Baja California [*Barton and Argote*, 1980; *Jeronimo and Gomez-Valdes*, 2006]. The standard error map also showed a coast-ocean gradient with the lowest variability at the coastal zone. This pattern is consistent with the dynamic height variability reported by *Lynn and Simpson* [1987], which is associated with the wind pattern. The variations of alongshore wind stress constrain the meridional orientation of the variability fields.

[39] The seasonal MLD changes off Baja California have been established. The maximum MLD occurred during

**Table 3.** Correlation Coefficient Between PC of the First Leading Mode of the Interannual MLD Anomalies and Climate Indices

| | Mixed Layer Depth |
|---|---|
| North Pacific Gyre Oscillation | −0.3 |
| Pacific Decadal Oscillation | 0.1 |
| Warm Water Volume | 0.4 |

January and the minimum during July. The one-dimensional model of *Kraus and Turner* [1967], which is based in the thermal energy equation, simulated very well the observations but only during the heating conditions (July), when entrainment is negligible [*Turner and Kraus*, 1967]. However, the one-dimensional model of *Pollard et al.* [1973], which is based in the momentum balance equation, simulated very well the MLD annual cycle. This model includes entrainment. *Lentz* [1992] found that this model explains MLD variations in coastal upwelling regions off Oregon, northwest Africa, Peru and northern California. However, here we found that at seasonal timescales the model correctly reproduces the MLD changes in the entire IMECOCAL domain (transitional and coastal).

[40] EOFs analysis of the quarterly anomalies reproduced the seasonal variability. The first leading mode revealed the temporal and spatial variability of the annual cycle. It was mainly correlated with the first leading mode of $\tau^y$ (offshore Ekman transport) in agreement with the results of the model of *Pollard et al.* [1973]. EOFs analysis of the interannual anomalies also revealed the major importance of offshore Ekman transport in the determination of MLD.

[41] *GVJ*2009 found that at interannual scales the first leading mode of both ML temperature and salinity was significantly correlated with ENSO. Here we found that the first leading mode of interannual MLD variability was also mainly correlated with ENSO, for example, an abrupt deepening of the pycnocline occurred from January 1998 to January 1999, and the strong 1997–1999 El Niño-La Niña cycle, intensified the variability from 1997 to 2000. *Durazo and Baumgartner* [2002] found a significant increase in volume of the California Undercurrent (warm and salty water). The deepening of the pycnocline in January 1998 would be associated to the deepening of the halocline due to the expansion of the California Undercurrent. In summary, we found more evidence that salinity variations control MLD variations not only at seasonal timescales but also at interannual timescales.

[42] **Acknowledgments.** This work has been supported in part by grants from CONACyT (Mexico) (82529, 23947), SEMARNAT-CONACyT (Mexico) (23804), and UNAM (Mexico) (PAPIIT IN-105305). We thank captain and crew of the R/V *Francisco de Ulloa* of CICESE. Special thanks go to Jorge Reyes de la Gala and Bernardo Gomez for their editorial review of the manuscript. We also thank two anonymous reviewers for their very helpful suggestions that improved the paper.

## References

Barton, E. D., and M. L. Argote (1980), Hydrographic variability in an upwelling area off northern Baja California in June 1976, *J. Mar. Res.*, *38*, 631–649.

Baumgartner, T., R. Durazo, B. Lavaniegos, G. Gaxiola, J. Gomez, and J. Garcia (2008), Ten years of change from IMECOCAL observations in the southern region of the California Current ecosystem, *GLOBEC Int. Newsl.*, *4*(2), 43–54.

Bograd, S. J., et al. (2000), The state of the California Current, 1999–2000: Forward to a new regime?, *Calif. Cooper. Oceanic Fish. Invest. Rep. 41*, pp. 26–52, Scripps Inst. of Oceanogr., La Jolla, Calif.

Brainerd, K. E., and M. C. Gregg (1995), Surface mixed and mixing layer depths, *Deep Sea Res.*, *42*, 1521–1543, doi:10.1016/0967-0637(95)00068-H.

Cummins, P. F., and G. S. E. Lagerloef (2002), Low-frequency pycnocline depth variability at Ocean Weather Station P in the northeast Pacific, *J. Phys. Oceanogr.*, *32*, 3207–3215, doi:10.1175/1520-0485(2002)032<3207:LFPDVA>2.0.CO;2.

de Boyer Montegut, C., G. Madec, A. S. Fisher, A. Lazar, and D. Iudicone (2004), Mixed layer depth over the global ocean: An examination of profile data and a profile-based climatology, *J. Geophys. Res.*, *109*, C12003, doi:10.1029/2004JC002378.

Di Lorenzo, E., et al. (2008), North Pacific Gyre Oscillation links ocean climate and ecosystem change, *Geophys. Res. Lett.*, *35*, L08607, doi:10.1029/2007GL032838.

Durazo, R., and T. R. Baumgartner (2002), Evolution of oceanographic conditions west of the Baja California: 1997–1999, *Prog. Oceanogr.*, *54*, 7–31, doi:10.1016/S0079-6611(02)00041-1.

Emery, W. J., and R. E. Thomson (2001), *Data analysis Methods in Physical Oceanography*, 2nd ed., 638 pp., Elsevier Sci., Amsterdam.

Freeland, H. J., K. Denman, C. S. Wong, F. Whitney, and R. Jacques (1997), Evidence of change in winter mixed layer in the northeast Pacific Ocean, *Deep Sea Res.*, *44*, 2117–2129, doi:10.1016/S0967-0637(97)00083-6.

Gomez-Valdes, J., and G. Jeronimo (2009), Upper mixed layer temperature and salinity variability in the tropical boundary of the California Current, 1997–2007, *J. Geophys. Res.*, *114*, C03012, doi:10.1029/2008JC004793.

Hasse, L., and S. D. Smith (1997), Local sea surface wind, wind stress and sensible and latent heat fluxes, *J. Clim.*, *10*, 2711–2724, doi:10.1175/1520-0442(1997)010<2711:LSSWWS>2.0.CO;2.

Jeronimo, G., and J. Gomez-Valdes (2006), Mean temperature and salinity along an isopycnal surface in the upper ocean off Baja California, *Cienc. Mar.*, *32*, 663–671.

Jeronimo, G., and J. Gomez-Valdes (2007), A subsurface warm-eddy off northern Baja California in July 2004, *Geophys. Res. Lett.*, *34*, L06610, doi:10.1029/2006GL028851.

Kara, A. B., P. A. Rochford, and H. E. Hurlburt (2000), An optimal definition for ocean mixed layer depth, *J. Geophys. Res.*, *105*(C7), 16,803–16,821, doi:10.1029/2000JC900072.

Kara, A. B., P. A. Rochford, and H. E. Hurlburt (2003), Mixed layer depth variability over the global ocean, *J. Geophys. Res.*, *108*(C3), 3079, doi:10.1029/2000JC000736.

Kim, H.-J., and A. J. Miller (2007), Did the thermocline deepen in the California Current after the 1976/77 climate regime shift?, *J. Phys. Oceanogr.*, *37*, 1733–1739, doi:10.1175/JPO3058.1.

Kraus, E. B., and J. S. Turner (1967), A one-dimensional model of the seasonal thermocline. II The general theory and its consequences, *Tellus*, *19*, 98–106.

Lentz, S. J. (1992), The surface boundary layer in coastal upwelling regions, *J. Phys. Oceanogr.*, *22*, 1517–1539, doi:10.1175/1520-0485(1992)022<1517:TSBLIC>2.0.CO;2.

Lukas, R., and E. Lindstrom (1991), The mixed layer of the western equatorial Pacific Ocean, *J. Geophys. Res.*, *96*, 3343–3358.

Lynn, R. J., and J. J. Simpson (1987), The California Current system: The seasonal variability of its physical characteristics, *J. Geophys. Res.*, *92*(C12), 12,947–12,966, doi:10.1029/JC092iC12p12947.

Mantua, N. J., S. R. Hare, Y. Zhang, J. M. Wallece, and R. C. Francis (1997), A Pacific interdecadal climate oscillation with impacts on salmon production, *Bull. Am. Meteorol. Soc. 78*, 1069–1079, doi:10.1175/1520-0477(1997)078<1069:APICOW>2.0.CO;2.

McPhaden, M. J. (1999), Genesis and evolution of the 1997–98 El Niño, *Science*, *283*, 950–954, doi:10.1126/science.283.5404.950.

Meinen, C. S., and M. J. McPhaden (2000), Observations of warm water volume changes in the equatorial Pacific and their relationship to El Niño and La Niña, *J. Clim.*, *13*, 3551–3559, doi:10.1175/1520-0442(2000)013<3551:OOWWVC>2.0.CO;2.

Moisan, J. R., and P. P. Niiler (1998), The seasonal heat budget of the North Pacific: Net heat flux and heat storage rates (1950–1990), *J. Phys. Oceanogr.*, *28*, 401–421, doi:10.1175/1520-0485(1998)028<0401:TSHBOT>2.0.CO;2.

Murphree, T., and C. Reynolds (1995), El Niño and La Niña effects on the northeast Pacific: The 1991–1993 and 1988–1989 events, *Calif. Cooper. Oceanic Fish. Invest. Rep. 36*, pp. 45–56, Scripps Inst. of Oceanogr., La Jolla, Calif.

Niiler, P. P., and E. B. Kraus (1977), One-dimensional models of the upper ocean, in *Modelling and Prediction of the Upper Layers of the Ocean*, edited by E. B. Kraus, pp. 143–172, Pergamon, Tarrytown, N. Y.

North, G. R., T. L. Bell, R. F. Cahalan, and F. J. Moeng (1982), Sampling errors in the estimation of empirical orthogonal functions, *Mon. Weather Rev.*, *110*, 699–706, doi:10.1175/1520-0493(1982)110<0699:SEITEO>2.0.CO;2.

Palacios, D. M., S. J. Bograd, R. Mendelssohn, and F. B. Schwing (2004), Long-term and seasonal trends in stratification in the California Current, 1950–1993, *J. Geophys. Res.*, *109*, C10016, doi:10.1029/2004JC002380.

Perez-Brunius, P., M. Lopez, A. Pares-Sierra, and J. Pineda (2007), Comparison of upwelling indices off Baja California derived from three

different wind data sources, *Calif. Cooper. Oceanic Fish. Invest. Rep. 48*, pp. 204–214, Scripps Inst. of Oceanogr., La Jolla, Calif.

Pollard, R. T., P. B. Rhines, and R. O. R. Y. Thompson (1973), The deepening of the wind-mixed layer, *Geophys. Fluid Dyn.*, *3*, 381–404.

Polovina, J. J., G. T. Mitchum, and G. T. Evans (1995), Decadal and basin-scale variation in mixed layer depth and the impact on biological production in the central and North Pacific, 1960–88, *Deep Sea Res.*, *42*, 1701–1716, doi:10.1016/0967-0637(95)00075-H.

Reid, J. L., G. I. Roden, and J. G. Wyllie (1958), Studies of the California Current system, *Calif. Cooper. Oceanic Fish. Invest. Rep. 6*, pp. 27–57, Scripps Inst. of Oceanogr., La Jolla, Calif.

Roden, G. I. (1975), On North Pacific temperature, salinity, sound velocity and density fronts and their relation to the wind and energy flux fields, *J. Phys. Oceanogr.*, *5*, 557–571, doi:10.1175/1520-0485(1975)005<0557:ONPTSS>2.0.CO;2.

Rudnick, D. L., and R. Ferrari (1999), Compensation of horizontal, temperature and salinity gradients in the ocean mixed layer, *Science*, *283*, 526–529, doi:10.1126/science.283.5401.526.

Salmon, R. (1998), *Lectures on Geophysical Fluid Dynamics*, 378 pp., Oxford Univ. Press, Oxford, U. K.

Schneider, N., and P. Müller (1990), The meridional and seasonal structures of the mixed-layer depth and its diurnal amplitude observed during the Hawaii-to-Tahiti Shuttle experiment, *J. Phys. Oceanogr.*, *20*, 1395–1404, doi:10.1175/1520-0485(1990)020<1395:TMASSO>2.0.CO;2.

Schwing, F. B., et al. (2002), The state of the California Current, 2001–2002: Will the California Current systems keep its cool, or is El Niño looming?, *Calif. Cooper. Oceanic Fish. Invest. Rep. 43*, pp. 31–68, Scripps Inst. of Oceanogr., La Jolla, Calif.

Sprintall, J., and M. Tomczak (1992), Evidence of the barrier layer in the surface layer of the tropics, *J. Geophys. Res.*, *97*(C5), 7305–7316, doi:10.1029/92JC00407.

Strub, P. T., and C. James (2000), Altimeter-derived variability of surface velocities in the California Current system: Part 2. Seasonal circulation and eddy statistics, *Deep Sea Res. Part II*, *47*, 831–870, doi:10.1016/S0967-0645(99)00129-0.

Turner, J. S., and E. B. Kraus (1967), A one-dimensional model of the seasonal thermocline. Part I. A laboratory experiment and its interpretation, *Tellus*, *19*, 88–97.

Wunsch, C., and P. Heimbach (2009), The global zonally integrated ocean circulation, 1992–2006: Seasonal and decadal variability, *J. Phys. Oceanogr.*, *39*, 351–368, doi:10.1175/2008JPO4012.1.

J. Gomez-Valdes, Physical Oceanography Department, CICESE, Km. 107 Carretera Tijuana-Ensenada, 22860 Ensenada, Baja California, Mexico. (jgomez@cicese.mx)

G. Jeronimo, UMDI-Sisal, Facultad de Ciencias, UNAM, Puerto de Abrigo S/N, 97355 Sisal, Yucatan, Mexico.